

Wavelet-based estimation of power densities of size-biased data*

Michel H. Montoril

Department of Statistics, Federal University of São Carlos, Brazil

e-mail: michel@ufscar.br

Aluísio Pinheiro

Department of Statistics, University of Campinas, Brazil

e-mail: pinheiro@ime.unicamp.br

and

Brani Vidakovic

Department of Statistics, Texas A&M University, USA

e-mail: brani@stat.tamu.edu

Abstract: We propose a new wavelet-based method for density estimation when the data are size-biased. More specifically, we consider a power of the density of interest, where this power exceeds $1/2$. Warped wavelet bases are employed, where warping is attained by some continuous cumulative distribution function. This can be seen as a general framework in which the conventional orthonormal wavelet estimation is the case where warping distribution is the standard uniform c.d.f. We show that both linear and nonlinear wavelet estimators are consistent, with optimal and/or near-optimal rates. Monte Carlo simulations are performed to compare four special settings which are easy to interpret in practice. An application with a real dataset on fatal traffic accidents involving alcohol illustrates the method. We observe that warped bases provide more flexible and superior estimates for both simulated and real data. Moreover, we find that estimating the power of a density (for instance, its square root) further improves the results.

MSC2020 subject classifications: Primary 62G07; secondary 62G20.

Keywords and phrases: Daubechies-Lagarias algorithm, density estimation, irregular design, size-biased data, warped wavelets.

1. Introduction

Frequently one may be interested in the probability density function (p.d.f.) f of some random variable (r.v.) X . The estimation of f is done based on a sample X_1, X_2, \dots, X_n , usually consisting of independent and identically distributed (i.i.d.) r.v.'s. In this scenario, there is a wide range of solutions [see, e.g. 20,

*The first author acknowledges FAPESP (Fundação de Amparo à Pesquisa do Estado de São Paulo) Grants 2018/04654-9 and 2020/00646-1. The second author acknowledges FAPESP Grant 2018/04654-9, and CNPq (Conselho Nacional de Desenvolvimento Científico e Tecnológico) Grant 310991/2020-0.

16, 30, 39]. Sometimes it may be impossible to collect such a sample. Rather, observing $X = x$ happens under the interference of some biasing device that imposes weights according to the magnitude (size) of x . In this situation one observes a sample Y_1, Y_2, \dots, Y_n of Y , which has p.d.f. g . This is a *biased sample* and its p.d.f. is related to f as

$$g(y) = \frac{w(y)f(y)}{\mu}, \quad (1)$$

where g is known to be the biased p.d.f., w is a weighting function, and $\mu = \mathbb{E}[w(X)]$.

The problem of biased data is introduced by [7], which proposes

$$\hat{F}(x) = \frac{\hat{\mu}}{n} \sum_{i=1}^n w^{-1}(Y_i) \mathbf{1}(Y_i \leq x)$$

as the estimator of the cumulative distribution function (c.d.f.) F , where $w^{-1}(y) = 1/w(y)$. $\mathbf{1}(A)$ is one, if A is true, and zero, otherwise. Moreover,

$$\hat{\mu} = \frac{n}{\sum_{i=1}^n w^{-1}(Y_i)}. \quad (2)$$

Since then, studies involving biased data have gained attention, especially because of their relevance to a wide range of applications. Consider the following example [16, 37]. We are interested in the distribution of the concentration of alcohol in the blood of intoxicated drivers. This data is usually available from routine police reports on arrested drivers charged with driving under the influence. Since more intoxicated drivers have increased chance of being arrested, the collected data are size-biased toward higher concentration of alcohol in the blood. Several other similar examples can be found on the literature. See, e.g. [17, 18, 37] and the references therein.

In terms of the estimation methodology, different approaches have been used to estimate f . For example, [43] considered a nonparametric maximum likelihood approach; [26] analyzed the mean square error properties of a kernel estimation method; [19] proposed a simple transformation approach; [18, 17] studied the asymptotic properties of f and F , respectively, via Fourier series; [2] considered projection estimator methods for right censored data; and [1] proposed bandwidth selection methods for the estimation of f when the kernel approach is used. Also, in the context of biased data, [42] proposed two approaches to test independence, both based on resampling methods.

In the density estimation problems, wavelet bases are strong competitors to other orthonormal bases, such as Fourier, Hermite etc. Wavelet bases are known to possess several optimality properties, such as adaptive simultaneous localization in space and scale/frequency, and have been used to solve several statistical problems. In the general density estimation context: [14, 15] introduce linear wavelet estimators; [27, 28] explore linear wavelet estimator in Besov spaces; [11, 12] consider nonlinear estimators and studies their minimax properties in

Besov spaces; [36] proposes the estimation based on the square root of the density, which is useful to control positiveness and L_1 -norm for the density estimate (the density estimate to integrate to 1); and [22] derives several uniform limits for the linear wavelet estimator.

Several studies have been developed on wavelet estimation of densities for biased data. Papers [37] and [6] consider wavelet-based methods to estimate the density of stratified biased data under the assumption of independent and associated data, respectively, and [8] derives asymptotic properties in L_2 -sense for linear and nonlinear wavelet-based estimators. Paper [23] exploits point-wise estimation, while [31] and [24] study the asymptotic properties of wavelet estimators for the density of multivariate (strong mixing and independent) biased data. Papers [46] and [47] consider the case of biased data with multiple change-points.

The novelty of the proposed approach is that we consider the estimation of the power density for biased data, say f^a , $a \geq 1/2$. The standard approach for the direct density estimation is a special case when the power is $a = 1$. Another special case we should mention is $a = 1/2$, considered by [36] for “unbiased” i.i.d. data. In the case of $a = 1/2$, one advantage when dealing with orthonormal bases is that projection estimators could be constructed to ensure non-negative density estimates that integrate to one (see the aforementioned reference for more details). Moreover, no L_2 assumption on f is required.

Another contribution of this paper is the use of warped wavelet bases in this context. This can be useful in stabilizing numerical estimates for finite data, specially in the regions with sparse observations, which is quite common given the biasing function. These warped wavelet bases provided good performance [34]. Some other references associated to warped wavelets are [3, 4, 29].

This paper is organized as follows. In Section 2 we propose and analyze the wavelet-based estimation method. Some theoretical results, special cases and computational aspects are discussed there. In Section 3, we evaluate the performance of the methodology, using four special cases, through Monte Carlo simulation studies and a real dataset application. Some comments and conclusions are made in Section 4. The proofs of the theoretical results are deferred to the Appendix A.

2. Wavelet-based estimator

2.1. A brief review of wavelets

Wavelet bases are systems of functions capable of an efficient and parsimonious representation of other square integrable functions. Specifically, any function $f \in L_2([0, 1])$ can be represented in $L_2([0, 1])$ -norm as

$$f(x) = \sum_{k \in \mathbb{Z}} c_{j_0 k} \phi_{j_0 k}(x) + \sum_{j=j_0}^{\infty} \sum_{k \in \mathbb{Z}} d_{jk} \psi_{jk}(x),$$

where $\phi_{j_0 k}(x) = 2^{j_0/2} \phi(2^{j_0} x - k)$ and $\psi_{jk}(x) = 2^{j/2} \psi(2^j x - k)$ are generated by the scaling ϕ , and embedded on a multiresolution analysis of $L_2([0, 1])$ [32]. ϕ is called the scaling function or father wavelet. ψ is called mother wavelet or simply wavelet, and it is also generated by ϕ .

Since we assume that f is defined on $[0, 1]$, we consider the periodized version of the wavelet bases, whose atoms can be written as

$$\phi_{jk}^p(x) = \sum_l \phi_{jk}(x - l), \quad \psi_{jk}^p(x) = \sum_l \psi_{jk}(x - l), \quad x \in [0, 1],$$

where $k = 0, \dots, 2^j - 1$, $j \in \mathbb{Z}$. One can show that, when $\{\phi_{jk}\}_k$ generates an orthonormal basis, then $\{\phi_{jk}^p\}_k$ will be orthonormal as well. Furthermore, if we consider compactly supported Daubechies wavelet bases, their periodized version shares most of their properties, with the advantage of dealing with the boundary problems [38]. In the sequel we adopt the periodized wavelets, and drop the superscript p for notational convenience. Thus, it is easy to see that shifts are bounded within the scales,

$$f(x) = \sum_{k=0}^{2^{j_0}-1} c_{j_0 k} \phi_{j_0 k}(x) + \sum_{j=j_0}^{\infty} \sum_{k=0}^{2^j-1} d_{jk} \psi_{jk}(x),$$

where the Fourier coefficients can be written as

$$c_{j_0 k} = \int_0^1 \phi_{j_0 k}(x) f(x) dx \quad \text{and} \quad d_{jk} = \int_0^1 \psi_{jk}(x) f(x) dx.$$

Let us now denote a -th power of f as $f^a(x) = [f(x)]^a$, $a \in \mathbb{R}$. Also, let h be the p.d.f. associated to the continuous c.d.f. H and take H^* as the inverse of H . Also, let us denote $r^a = f^a \circ H^*$ and $y = H(x)$, $x \in [0, 1]$. Then,

$$\begin{aligned} f^a(x) &= f^a(H^*(H(x))) \equiv r^a(y) \\ &= \sum_{k=0}^{2^{j_0}-1} c_{j_0 k} \phi_{j_0 k}(y) + \sum_{j \geq j_0} \sum_{k=0}^{2^j-1} d_{jk} \psi_{jk}(y) \\ &= \sum_{k=0}^{2^{j_0}-1} c_{j_0 k} \phi_{j_0 k}[H(x)] + \sum_{j \geq j_0} \sum_{k=0}^{2^j-1} d_{jk} \psi_{jk}[H(x)]. \end{aligned} \tag{3}$$

The wavelet basis in (3) is “warped” by H , and the expansion can be seen as a generalization of the ordinary wavelet analysis. Observe that, when $H(x) = x$, (3) reduces to the usual case. Furthermore, as discussed in Section 1, this warped representation may be advantageous for statistical analyses of irregularly spaced data [34].

2.2. Linear wavelet-based estimation

We consider f^a , $a \geq 1/2$ for the size-biased data problem, where f is defined as in (1). Assuming that $f \in L_{2a}([0, 1])$ (or, equivalently, $f^a \in L_2([0, 1])$), f^a

can be approximated by its orthogonal projection on some multiresolution space V_{J_0} , say $f_{J_0}^a$, for any arbitrary resolution level J_0 , which results in

$$f_{J_0}^a(x) = \sum_{k=0}^{2^{J_0}-1} c_{J_0k} \phi_{J_0k}[H(x)]. \quad (4)$$

The Fourier coefficients satisfy

$$\begin{aligned} c_{J_0k} &= \langle f^a \circ H^*, \phi_{J_0k} \rangle = \int_0^1 \phi_{J_0k}[H(x)] \frac{\mu^a g^a(x)}{w^a(x)} h(x) dx \\ &= \mu^a \mathbb{E} \left\{ \frac{\phi_{J_0k}[H(Y)] g^{a-1}(Y)}{w^a(Y) h(Y)} \right\}, \end{aligned} \quad (5)$$

where $k = 0, 1, \dots, 2^{J_0} - 1$.

Based on (5), the coefficients could be estimated by moment matching, resulting in

$$\bar{c}_{J_0k} = \frac{\mu^a}{n} \sum_{i=1}^n \frac{\phi_{J_0k}[H(Y_i)] g^{a-1}(Y_i) h(Y_i)}{w^a(Y_i)}.$$

Such estimator is not useful in practical situations because both μ and g are unknown. This problem can be solved by plugging-in their estimates. Observe that g can be easily estimated from the biased data. Kernel-based and wavelet-based estimators are just two efficient methodologies. Let us denote this estimator by \hat{g} . We can use $\hat{\mu}$ as defined by (2). Therefore, the linear wavelet estimator of f^a can be written as

$$\begin{aligned} \hat{f}_{J_0}^a(x) &= \sum_{k=0}^{2^{J_0}-1} \hat{c}_{J_0k} \phi_{J_0k}[H(x)], \\ \hat{c}_{J_0k} &= \frac{\hat{\mu}^a}{n} \sum_{i=1}^n \frac{\phi_{J_0k}[H(Y_i)] \hat{g}^{a-1}(Y_i) h(Y_i)}{w^a(Y_i)}. \end{aligned} \quad (6)$$

One can then estimate f by

$$\hat{f}_{J_0}(x) = \left[\hat{f}_{J_0}^a(x) \right]^{1/a}. \quad (7)$$

2.3. Regularized wavelet-based estimation

The choice of the resolution level J_0 is a well-known problem in statistical analysis by wavelets [see, e.g. 44, 35, for details]. Larger values of J_0 lead to larger variances, whilst smaller values yield fewer coefficients leading to oversmoothing. Balancing bias and variance may be attained by employing more detail coefficients. Regularization of these “extra” coefficients helps reducing oversmoothing

and providing adaptive estimates. We consider a projection on V_{J_1} :

$$f_{J_1}^a(x) = \sum_{k=0}^{2^{J_0}-1} c_{J_0 k} \phi_{J_0 k}[H(x)] + \sum_{j=J_0}^{J_1-1} \sum_{k=0}^{2^j-1} d_{jk} \psi_{jk}[H(x)] \quad (8)$$

$$= f_{J_0}^a(x) + \sum_{j=J_0}^{J_1-1} \sum_{k=0}^{2^j-1} d_{jk} \psi_{jk}[H(x)]. \quad (9)$$

Analogously to (5), one has

$$d_{jk} = \mu^a \mathbb{E} \left\{ \frac{\psi_{jk}[H(Y)] g^{a-1}(Y) h(Y)}{w^a(Y)} \right\}, \quad (10)$$

$k = 0, 1, \dots, 2^j - 1$, $j = J_0, \dots, J_1 - 1$. The detail coefficients can be estimated as

$$\hat{d}_{jk} = \frac{\hat{\mu}^a}{n} \sum_{i=1}^n \frac{\psi_{jk}[H(Y_i)] \hat{g}^{a-1}(Y_i) h(Y_i)}{w^a(Y_i)}.$$

We shrink \hat{d}_{jk} by

$$\hat{d}_{jk}^* = \lambda_{jk} \hat{d}_{jk},$$

where $0 \leq \lambda_{jk} \leq 1$ plays the role of thresholding regularizer. There are several regularization methods that satisfy this representation. Two of the most famous are the hard- and the soft-thresholding approaches, where the latter is written as $\hat{d}_{jk}^* = \text{sign}(\hat{d}_{jk})(|\hat{d}_{jk}| - \lambda)_+$, and the former satisfies $\hat{d}_{jk}^* = \hat{d}_{jk} \mathbb{1}(|\hat{d}_{jk}| > \lambda)$. See [44] for details.

The proposed regularized nonlinear wavelet estimator is then given by

$$\tilde{f}_{J_1}^a(x) = \hat{f}_{J_0}^a(x) + \sum_{j=J_0}^{J_1-1} \sum_{k=0}^{2^j-1} \hat{d}_{jk}^* \psi_{jk}[H(x)]. \quad (11)$$

We show in Section 2.4 that proposals (6) and (11) both result in consistent estimators.

2.4. Theoretical results

In this section we discuss the mean integrated square error (MISE) consistency of $\hat{f}_{J_0}^a$ and $\tilde{f}_{J_1}^a$. For instance, we say that \hat{f}_J is MISE-consistent estimating f if $\lim_n \mathbb{E} \|\hat{f}_J - f\|_2 = 0$, where $\|h\|_p = \left(\int_0^1 h^p(x) dx \right)^{1/p}$, $1 \leq p < \infty$.

Usually f possess some degree of smoothness. Specifically we assume that f belongs to a Sobolev space.

Definition 1. Let $m \in \{0, 1, \dots\}$ and $1 \leq p \leq \infty$. The Sobolev space corresponds to the set of functions $W_p^m([0, 1]) = \{f \in L_p([0, 1]) : f^{(m)} \in L_p([0, 1])\}$. It is equipped with the norm $\|f\|_{W_p^m} = \|f\|_p + \|f^{(m)}\|_p$.

Let us focus on the Sobolev ball

$$\tilde{W}_p^m(U) = \left\{ f \in W_p^m([0, 1]) : f \text{ is a p.d.f., } \|f^{(m)}\|_p \leq U \right\}.$$

This class of functions is similar, for example, to the class used by [25] (Theorem 10.1) or [45].

Further, we impose some regularity conditions. First some notation is required. For two sequences of positive numbers a_n and b_n , we say that $a_n \lesssim b_n$, if the ratio is uniformly bounded, and $a_n \asymp b_n$, if $a_n \lesssim b_n$ and $b_n \lesssim a_n$.

Assumptions

- (a1) f in (1) is bounded away from zero and infinity and $f^a \in \tilde{W}_2^m(U)$, for $a \geq 1/2$, $0 < U < \infty$ and $m = 1, 2, \dots$
- (a2) w in (1) is bounded away from zero and infinity.
- (a3) The c.d.f. H used to warp the wavelet basis is continuous and strictly monotone. Its p.d.f. h is bounded away from zero and infinity uniformly on $[0, 1]$.
- (a4) The employed wavelet basis is a periodized version of some Daubechies compactly supported wavelet basis, with at least m vanishing moments.

The above assumptions are frequently used in the literature. For example, (a2) is used in [17, 18, 45] and (a3) is considered by [34].

Remark 1. The assumptions (a1) and (a2) ensure that g in (1) is also bounded away from zero and infinity.

Remark 2. The proofs of the results presented here are available in the Appendix A.

Theorem 1. Suppose assumptions (a1) – (a4) hold. Furthermore, assume that $J_0 \equiv J_0(n)$ is an increasing sequence of positive integers such that $2^{J_0}/n \rightarrow 0$. Then, for $a = 1$, $\hat{f}_{J_0}^a$ in (6) is MISE-consistent. Its rate of convergence is given by

$$\sup_{f^a \in \tilde{W}_2^m(U)} \mathbb{E} \|\hat{f}_{J_0}^a - f^a\|_2^2 \lesssim \frac{2^{J_0}}{n} + 2^{-2mJ_0}.$$

Theorem 1 states that the use of warping wavelets in the conventional case ($a = 1$) does not impact the minimax rate of convergence. Therefore, the rate of convergence will be minimized if we consider $2^{J_0} \asymp n^{\frac{1}{2m+1}}$. In this case, one can see that

$$\sup_{f^a \in \tilde{W}_2^m(U)} \mathbb{E} \|\hat{f}_{J_0}^a - f^a\|_2^2 \lesssim n^{-\frac{2m}{2m+1}}.$$

Theorem 2. Suppose assumptions (a1) – (a4) hold. Furthermore, assume that $J_0 \equiv J_0(n)$ is an increasing sequence of positive integers. If there exists a positive sequence D_n such that $2^{J_0} D_n \rightarrow 0$ as $n \rightarrow \infty$ and $\sup_{y \in [0, 1]} |\hat{g}(y) - g(y)|^2 \lesssim D_n$,

then for $a \neq 1$, $\hat{f}_{J_0}^a$ given by (6) is MISE-consistent. Its rate of convergence will be

$$\sup_{f^a \in \tilde{W}_2^m(U)} \mathbb{E} \|\hat{f}_{J_0}^a - f^a\|_2^2 \lesssim 2^{J_0} D_n + \frac{2^{J_0}}{n} + 2^{-2mJ_0}.$$

Theorem 2 states that the rate of convergence will no longer be minimax when we consider a non-trivial power of f . As expected, the rate of convergence is slower. This happens because the estimators of the coefficients $c_{J_0 k}$ in (6) depend on another estimator, specifically \hat{g} . We need not only convergence of $\hat{c}_{J_0 k}$ to $c_{J_0 k}$, but the sup-norm convergence between \hat{g} and g as well.

We should also note regarding Theorem 2 that its stated MISE-consistency depends on $2^{J_0} D_n \rightarrow 0$ as $n \rightarrow \infty$, where D_n is \hat{g} 's rate of convergence. One finds several sup-norm convergence results for kernel density estimators [41, 21] and wavelet-based estimators, for both linear and nonlinear approaches [22].

We illustrate this issue by considering \hat{g} a linear wavelet-based estimator with some resolution level j_n , i.e.,

$$\begin{aligned} \hat{g}(x) &= \sum_{k=0}^{2^{j_n}-1} \hat{\alpha}_{j_n k} \phi_{j_n k}(x), \\ \hat{\alpha}_{j_n k} &= \frac{1}{n} \sum_{i=1}^n \phi_{j_n k}(Y_i). \end{aligned} \tag{12}$$

The resolution level j_n is assumed to be an increasing sequence of n that satisfies

$$\frac{j_n 2^{j_n}}{n} \rightarrow 0, \quad \frac{\log \log n}{n} \rightarrow 0 \quad \text{and} \quad \sup_{n \geq n_0} (j_{2n} - j_n) \leq \tau \tag{13}$$

for some $\tau \geq 1$ and some $n_0 < \infty$. The necessary conditions for Theorem 2 to hold are guaranteed by Theorem 3.

Theorem 3 ([22]). *Suppose that $g \in W_2^m([0, 1])$. If the assumptions (13) and (a4) hold, then*

$$\sup_y |\hat{g}(y) - g(y)| \lesssim \sqrt{\frac{j_n 2^{j_n}}{n}} + 2^{-mj_n}.$$

The original version of Theorem 3 is more general, and g is considered to live in a Besov space. This is not an issue here because Sobolev spaces are covered as well. See [22] Remarks 3 and 8 for details. If we take $j_n = J_0$ Corollary 1 summarizes the consistency results for linear warped wavelet estimators.

Corollary 1. *Suppose assumptions (a1) – (a4). Furthermore, assume that $J_0 \equiv J_0(n)$ is an increasing sequence of positive integers satisfying (13) and $J_0 2^{2J_0}/n \rightarrow 0$. If g satisfies suppositions in Theorem 3, then for $a \neq 1$, $\hat{f}_{J_0}^a$ given by (6) is MISE-consistent. Its rate of convergence is given by*

$$\sup_{f^a \in \tilde{W}_2^m(U)} \mathbb{E} \|\hat{f}_{J_0}^a - f^a\|_2^2 \lesssim \frac{J_0 2^{2J_0}}{n} + 2^{-(2m-1)J_0}.$$

The rate of convergence above will be optimal if $2^{J_1} \asymp (n/\log n)^{1/(2m+1)}$, where

$$\sup_{f^a \in \tilde{W}_2^m(U)} \mathbb{E} \|\hat{f}_{J_0}^a - f^a\|_2^2 \lesssim \left(\frac{\log n}{n} \right)^{\frac{2m-1}{2m+1}}.$$

Theorems 4 and 5 state that it is possible for nonlinear warped wavelet estimators to attain the same MISE convergence rates obtained in Theorems 1 and 2 (and Corollary 1) for linear warped wavelet estimators.

Theorem 4. *Suppose assumptions (a1) – (a4). Furthermore, assume that $J_0 \equiv J_0(n)$ and $J_1 \equiv J_1(n)$ are increasing sequences of positive integers such that $J_0 \leq J_1$, $2^{J_0} \asymp 2^{J_1}$ and $2^{J_1}/n \rightarrow 0$. Then, for $a = 1$, $\hat{f}_{J_1}^a$ given by (11) is MISE-consistent. Its rate of convergence is*

$$\sup_{f^a \in \tilde{W}_2^m(U)} \mathbb{E} \|\tilde{f}_{J_1}^a - f^a\|_2^2 \lesssim \frac{2^{J_1}}{n} + 2^{-2mJ_1}.$$

Theorem 5. *Suppose assumptions (a1) – (a4). Furthermore, assume that $J_0 \equiv J_0(n)$ and $J_1 \equiv J_1(n)$ are increasing sequences of positive integers such that $J_0 \leq J_1$, $2^{J_0} \asymp 2^{J_1}$, and there exists a positive sequence D_n such that $2^{J_1} D_n \rightarrow 0$, as $n \rightarrow \infty$, with $\sup_{y \in [0,1]} |\hat{g}(y) - g(y)|^2 \lesssim D_n$. If g satisfies Theorem 3, then for $a \neq 1$, $\hat{f}_{J_1}^a$ given by (11) is MISE-consistent. Its rate of convergence is given by*

$$\sup_{f^a \in \tilde{W}_2^m(U)} \mathbb{E} \|\tilde{f}_{J_1}^a - f^a\|_2^2 \lesssim 2^{J_1} D_n + \frac{2^{J_1}}{n} + 2^{-2mJ_1}.$$

Corollary 2. *Suppose assumptions (a1) – (a4) hold. Furthermore, assume that $J_0 \equiv J_0(n)$ and $J_1 \equiv J_1(n)$ are increasing sequences of positive integers such that $J_0 \leq J_1$, $2^{J_0} \asymp 2^{J_1}$ and $J_1 2^{2J_1}/n \rightarrow 0$. If g behaves as stated in Theorem 3, then for $a \neq 1$, $\hat{f}_{J_1}^a$ given by (11) is MISE-consistent. Its rate of convergence is given by*

$$\sup_{f^a \in \tilde{W}_2^m(U)} \mathbb{E} \|\tilde{f}_{J_1}^a - f^a\|_2^2 \lesssim \frac{J_1 2^{2J_1}}{n} + 2^{-(2m-1)J_1}.$$

It is usual in the literature to demonstrate that nonlinear wavelet-based estimators are asymptotically minimax up to a logarithmic term [see, e.g. 12], where the finest resolution level does not depend on unknown quantities such as regularity parameters of function spaces. In practice, as mentioned by [22], one can choose J_1 sufficiently large (and independent of m) and regularize by shrinking or thresholding selected wavelet coefficient estimates in resolution levels from J_0 to J_1 . In the case of the regularized wavelet estimators proposed here, when $a = 1$, assumption (a3) ensures that the adaptive rate of convergence for the nonlinear warped estimator can be easily derived based on results known in the literature (under similar arguments presented in (19), proof of Theorem 2). An adaptive rate that could be taken into account is presented in Theorem 4.1 of [5], where the author consider a block thresholding approach. The case where $a \neq 1$ is more problematic. Observe that the rate of convergence in Theorem 5

depends on the sequence D_n , which is quite generic and makes the development of the results unfeasible. Even in specific situations, such as the one illustrated in Corollary 1, the assumptions necessary to derive adaptive rates of convergence tend to be unrealistic.

By the arguments presented above, we simply focus on showing that the proposed nonlinear wavelet estimators (11) are still MISE-convergent, although not in an adaptive way. Therefore, Theorems 4 and 5 guarantee that the regularized warped wavelet estimators can both rely on a sparse representation and attain the same rates of convergence as their linear versions, where the optimal rate of the former still depend on resolution levels which, in sequel, depend on the regularity parameter m . In practice, this can be seen as a drawback, because m is unknown. On the other hand, one can easily perform an empirical analysis to estimate the finest resolution level. We illustrate it for Theorem 4 and Corollary 2.

Let us focus initially on the case where $a = 1$. Denote by $R_m^k(n)$ the rate of convergence of $\sup_{f^a \in \tilde{W}_2^m(U)} \mathbb{E} \|\tilde{f}_{J_1}^a - f^a\|_2^2$, in the case where one chooses $2^{J_1} \asymp n^{\frac{1}{2k+1}}$. Thus, one can see that $R_m^k(n) = n^{-2(k \wedge m)/(2k+1)}$. Observe that $R_m^m(n) \lesssim n^{-2m/(2m+1)}$. Therefore, it is possible to compare the performance of a “bad” choice of resolution level with respect to the optimal rate. In this case, let us denote $\text{eff}(k, m) = R_m^k(n)/R_m^m(n) = n^{-2(k \wedge m)/(2k+1) + 2m/(2m+1)}$, which play the role of a kind of asymptotic relative efficiency. For the case where $a \neq 1$, one can consider the choice of $2^{J_1} \asymp (n/\log n)^{\frac{1}{2k+1}}$ and obtain $R_m^k(n) = ((\log n)/n)^{\frac{2(k \wedge m)-1}{2k+1}}$, which provides $\text{eff}(k, m) = ((\log n)/n)^{\frac{2(k \wedge m)-1}{2k+1} - \frac{2m-1}{2m+1}}$.

The asymptotic relative efficiencies based on Theorems 4 and 5 are presented in Figure 1. In the case where $a = 1$, one can see that, for choices of $k \leq m$ the efficiency is closer to one, and it increases fast for choices of $k > m$. On the other hand, in the case where $a \neq 1$, smaller values of k are interesting when the f^a is not too regular (m small). The more regular f^a becomes (greater values of m), the choice $k = 1$ tends to increase $\text{eff}(1, m)$. Therefore, $k = 2$ or $k = 3$ seem to be good candidates to provide nearly optimal rates of convergence.

2.5. A few special cases

There are infinitely many estimators for the density f based on (6), because of many choices for the power a and the warping function H . When $H(x) = x$, $0 < x < 1$, the case where $a = 1$ represents the standard estimator, frequently explored [see, e.g. 37, 8]. Still in the case of an identity warping function, $a = 1/2$ can be seen as a natural generalization of [36] to the context of biased data. On the other hand, one can explore the possibility of warping the wavelet basis, taking into account some different function H . This can be seen as an attempt to improve the estimates, specially in regions where the weighting function is closer to zero. An interesting case corresponds to $H(x) = G(x)$, i.e., we consider the c.d.f. of the biased data. Since, as mentioned before, G (and, consequently, g) is unknown, we need to estimate it. A natural candidate is the empirical c.d.f., which we denote by \hat{G} . With respect to h , a natural candidate is \hat{g} , the

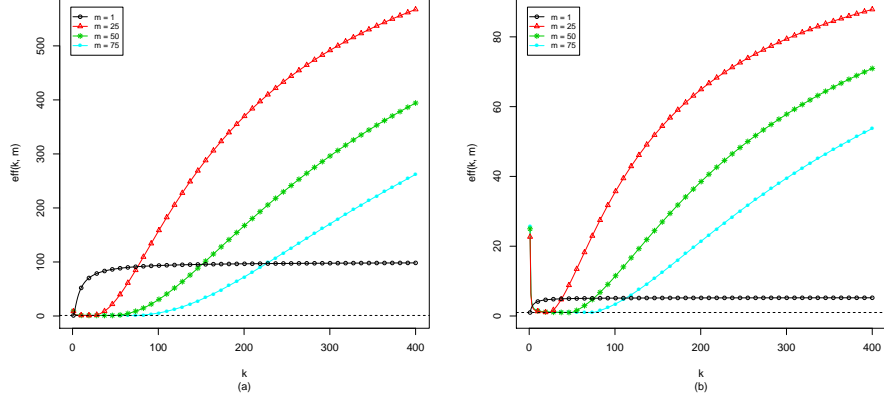


FIG 1. Relative efficiency (Theorem 4 and Corollary 2) $\text{eff}(k, m)$, for $1 \leq k \leq 400$, using $n = 1000$ and the regularity parameter $m = 1, 25, 50, 75$. The horizontal dashed line is a reference where $\text{eff}(k, m) = 1$. Figures (a) and (b) correspond to the $\text{eff}(k, m)$ in the cases $a = 1$ and $a \neq 1$, respectively.

same estimator employed for g . Therefore, the wavelet coefficient estimator in (6) becomes

$$\hat{c}_{J_0 k} = \frac{\hat{\mu}^a}{n} \sum_{i=1}^n \frac{\phi_{J_0 k} [\hat{G}(Y_i)] \hat{g}^a(Y_i)}{w^a(Y_i)}.$$

In this work we consider four cases to be explored. These methods of estimation correspond to

- \mathbf{m}_1 : when $a = 1/2$ and $H(x) = x$;
- \mathbf{m}_2 : when $a = 1$ and $H(x) = x$;
- \mathbf{m}_3 : when $a = 1/2$ and $H(x) = \hat{G}(x)$;
- \mathbf{m}_4 : when $a = 1$ and $H(x) = \hat{G}(x)$.

The procedure of regularization is analogous to that discussed in Section 2.3. Hereafter, we refer to m_k , $k = 1, 2, 3, 4$, as the regularized method.

2.6. Computational aspects

In the real world the range of data is seldom the unit interval. We briefly discuss here how we employ the proposed wavelet estimators the domain is arbitrary. For appropriate q and s , take $Y^\circ = (Y - q)/s$ and $X^\circ = (X - q)/s$, with densities g_{Y° and f_{X° , respectively. Hence, it is easy to see that $f(x) = f_{X^\circ}((x - q)/s)/s$

and, after some algebra, one can derive

$$\begin{aligned}\hat{f}_{J_0}(x) &= \frac{1}{s} \left[\hat{f}_{X^\circ}^a(x^\circ) \right]^{1/a}, \\ \hat{f}_{X^\circ}^a(x^\circ) &= \sum_{k=0}^{2^{J_0}-1} \hat{c}_{J_0 k}^\circ \phi_{J_0 k} [H(x^\circ)], \\ \hat{c}_{J_0 k}^\circ &= \frac{\hat{\mu}^a}{n} \sum_{i=1}^n \frac{\phi_{J_0 k} [H(Y_i^\circ)] \hat{g}_{Y^\circ}^{a-1}(Y_i^\circ) h(Y_i^\circ)}{w^a(Y_i)}.\end{aligned}$$

It is important to mention that $\hat{\mu}$ and w are associated with Y_i 's, and not with Y_i° 's.

The periodized wavelets impose a periodic analysis to the function of interest. Therefore, a solution is transforming the data into $[\epsilon, 1 - \epsilon]$, for some $0 \leq \epsilon < 1$. We denote the ordered sample $y_{(1)} < y_{(2)} < \dots < y_{(n)}$, and $r = y_{(n)} - y_{(1)}$. The adequate constants are given then by $q = y_{(1)} - \epsilon r / (1 - 2\epsilon)$ and $s = r$. Following [33], we consider $\epsilon = 1.9^{-J_1}$.

Remark 3. *The transformation of the data, as described above, has impact only in the cases where the wavelet bases are not warped. In fact, the empirical c.d.f. will always be k/n , $k = 1, \dots, n$, for the observed sample.*

Regularization is performed analogously to Section 2.3.

3. Numerical studies

We present now some Monte Carlo simulations as well as a real data application. The dataset is not equally spaced. Since, except for the Haar basis, compactly supported orthonormal wavelets do not possess analytic expressions, we need some numerical interpolation. We employ the Daubechies-Lagarias algorithm [9, 10], which can attain any preassigned precision [see, e.g. 44]. Analyses are performed with Symmlets S10 (Daubechies least asymmetric 20-tap filter).

We consider methods of estimation m_k , $k = 1, 2, 3, 4$, as presented in Section 2.5. This gives us an idea of how the density's square root estimate ($a = 1/2$) can improve the ordinary approach ($a = 1$), as well as if a warped wavelet basis can provide a better performance. For the methods m_1 and m_3 , we estimate g by a Gaussian kernel with bandwidth selected according to [40]. For the methods m_3 and m_4 , the wavelet basis is warped by the empirical c.d.f. of the data, linearly interpolated.

Regularization is done by the universal hard threshold, i.e., $\lambda = \hat{\sigma} \sqrt{2 \log 2^{J_1-1}}$, where $\hat{\sigma}$ is the median absolute deviation of the detail coefficients in the finest resolution level [13].

3.1. Simulation studies

The performance of the estimation methods is evaluated by Monte Carlo simulation studies. For such a task, we consider three different examples described

below.

Example 1. We assume that $X \sim \text{Beta}(2.5, 2.5)$ and $w(y) = y^{-2}(1 - y)^{-2}$. In this case, $Y \sim \text{Beta}(0.5, 0.5)$. Therefore, the shapes of f and g are “inverted”, as it can be observed in the first row of Figure 2. \square

Example 2. Let us denote by $\beta(x, a, b)$ the density of a beta with parameters a and b evaluated at x . Thus, in this example we consider a mixture of three betas for the density of interest:

$$f(x) = (1/3)\beta(x, 20, 3) + (1/3)\beta(x, 40, 40) + (1/3)\beta(x, 3, 20).$$

The weighting function is $w(y) = y$. This results in a biased sample from the density

$$g(y) = (40/69)\beta(y, 21, 3) + (1/3)\beta(y, 41, 40) + (2/23)\beta(y, 4, 20).$$

In this example, the biased density remains a mixture of betas, but now with “unbalanced” weights, as presented in the second row of Figure 2. \square

Example 3. In this example we consider a piecewise linear density for f , where

$$f(x) = \begin{cases} \frac{64x + 1}{32}, & 0 \leq x < 0.25, \\ \frac{9}{32(1 - 2x) + 1}, & 0.25 \leq x < 0.5, \\ \frac{x(32x - 31) + 12}{9}, & 0.5 \leq x < 0.75, \\ \frac{x(65 - 32x) - 24}{9}, & 0.75 \leq x \leq 1. \end{cases}$$

As biasing function, we employed in this example $w(y) = 0.1 + 2x^2$. We do not present the cumbersome resulting biased density of Y . However, it can be seen in the third row of Figure 2 that the biased density presents a different shape (still not smooth, but no longer piecewise linear). This provides a challenge to estimate f . Data values are numerically generated by accept-reject algorithm [16, Section 3.6]. \square

The examples above will be denoted hereafter by ex_1 , ex_2 and ex_3 . We generate 1,000 biased samples with sizes $n = 250, 500, 750, 1000$. For the finest resolution level, we consider the cases $J_1 = \lceil p \log_2 n \rceil$, where $p = 0.20, 0.45, 0.70, 0.95$ and $\lceil x \rceil$ represents the smallest integer greater than or equal to x . We adopt as coarsest resolution level $J_0 = 0$.

We numerically evaluate the estimate’s closeness to the real function of interest by the average square error (ASE), defined as

$$\text{ASE}(\hat{f}, f) = \frac{1}{n} \sum_{i=1}^{n_{\text{grid}}} [\hat{f}(x_i) - f(x_i)]^2,$$

where $x_1, \dots, x_{n_{\text{grid}}}$ correspond to a grid of $n_{\text{grid}} = 250$ equally spaced points inside the unit interval. Since we have 1,000 samples for each sample size, data

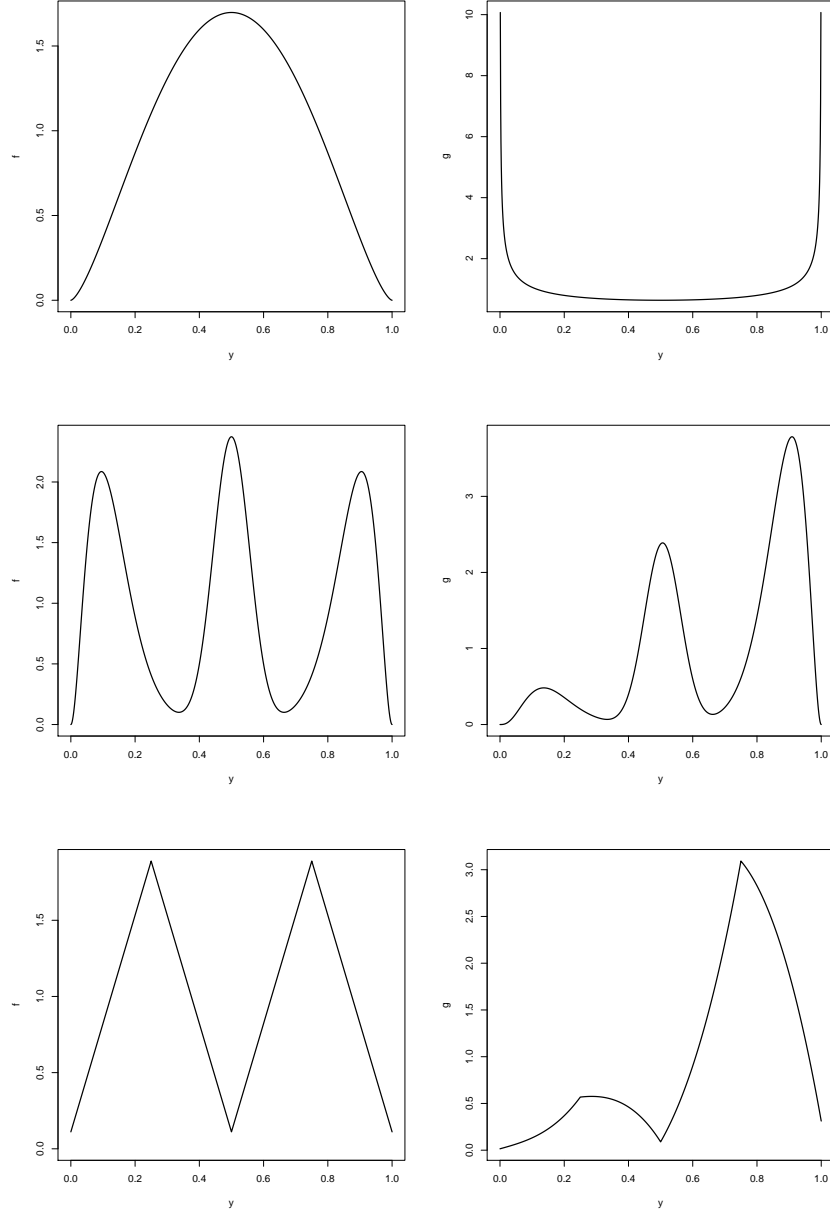


FIG 2. Densities used in the simulations (Examples ex_1 - ex_3). The first and second columns represent the densities f and g , respectively. The i -th row corresponds to the simulation example ex_i , $i = 1, 2, 3$.

range vary. In order to make the ASEs comparable, we consider the maximum among the minimums and the minimum of the maximums of the datasets to represent x_1 and $x_{n_{\text{grid}}}$, respectively.

Performance of the finest resolution level's candidates can be observed in Figure 3. For m_1 and m_2 (ordinary wavelet basis), these methods tend to provide poor estimates for larger values of J_1 ($p = 0.70$ and 0.95). In ex_1 , $p = 0.20$ show a performance slightly superior to $p = 0.45$. On the other hand, one sees considerable improvement when changing from $p = 0.20$ to $p = 0.45$ for ex_2 . Finally, in ex_3 , $p = 0.45$ tends to provide a slight improvement for the estimates, when compared to $p = 0.20$. This suggests that $J_1 = \lceil 0.45 \log_2 n \rceil$ seems to be a good choice for the finest level. Furthermore, when comparing these two methods, m_1 presents the worst estimates, with greater mean and variability, sometimes providing negative density estimates.

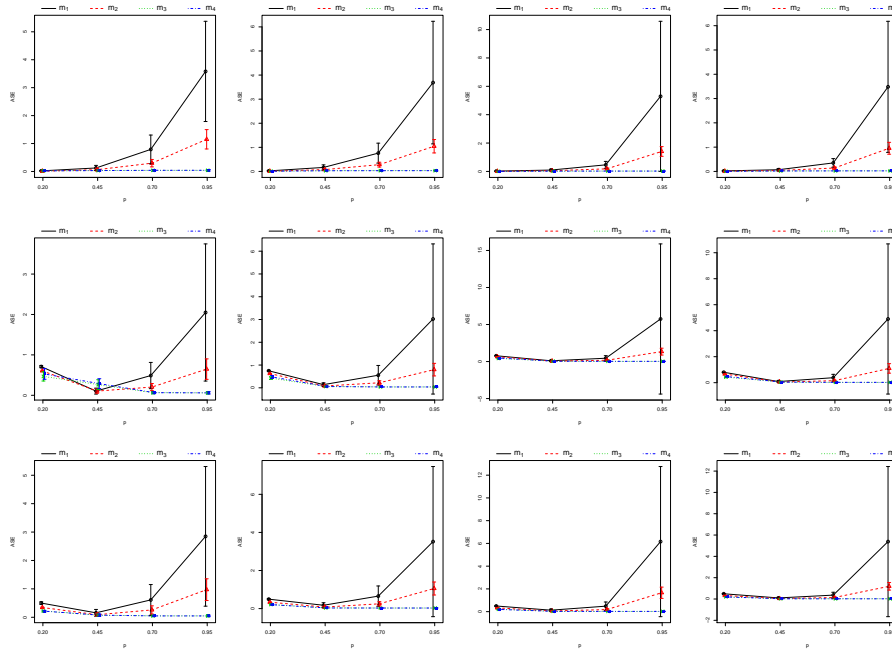


FIG 3. Average plus/minus a standard deviation of the ASEs. The full lines, dashed lines, dotted lines and dot-dashed lines represent the ASEs obtained by the methods m_1 – m_4 , respectively. Columns 1–4 are related to the datasets with sample sizes $n = 250, 500, 750, 1000$, respectively. The i -th row corresponds to the example i , $i = 1, 2, 3$.

We also see in Figure 3 that the estimates obtained by warped wavelet basis (m_3 and m_4) present an opposite behavior to m_1 and m_2 . Larger values of J_1 yield in general better estimates. This suggests that the finest resolution level for $J_1 = \lceil 0.95 \log_2 n \rceil$ is a good alternative for methods of estimation based on the warped basis. Moreover, the estimates of m_3 and m_4 look very similar (almost equal). Finally, one can see that the warped basis provide an improvement on

the estimates, with average ASEs closer to zero as well as smaller standard deviations.

Figure 4 presents the estimator's performance for fixed resolution levels, as sample size increases. In general, one can see that all the four methods of estimation provide estimates that converge to the density of interest. One clear exception corresponds to the case where $J_1 = \lceil 0.20 \log_2 n \rceil$ in ex_2 . This reinforces that such a resolution level is not indicated, which is inline with some arguments above for Figure 3. Also, one can clearly see the superiority of estimates based on warped wavelets, which provide ASEs with smaller averages and standard deviations.

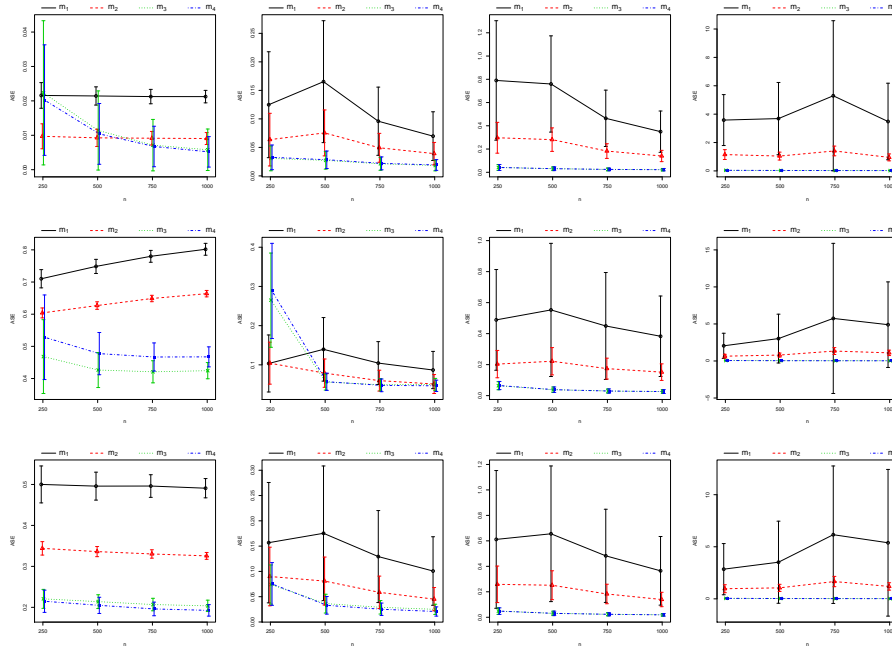


FIG 4. Average plus/minus a standard deviation of the ASEs. Full lines, dashed lines, dotted lines and dot-dashed lines represent the ASEs obtained by the methods m_1 – m_4 , respectively. Columns 1–4 are related to the cases where we consider the finest resolution level $J_1 = \lceil p \log_2 n \rceil$, $p = 0.20, 0.45, 0.70, 0.95$, respectively. The i -th row corresponds to the example i , $i = 1, 2, 3$.

Finally, another advantage of using warped wavelets can be observed in Figures 5–7, which present pointwise estimates (averages) and 95% confidence intervals (highest density intervals) based on the 1,000 replications. It becomes clear that estimates based on warped wavelets are more precise for regions in the density's support where the weighting function is close to zero. Furthermore, poor estimates are obtained for all methods m_k , $k = 1, 2, 3, 4$. When we employ $J_1 = \lceil 0.95 \log_2 n \rceil$, the traditional method m_2 is providing negative estimates.

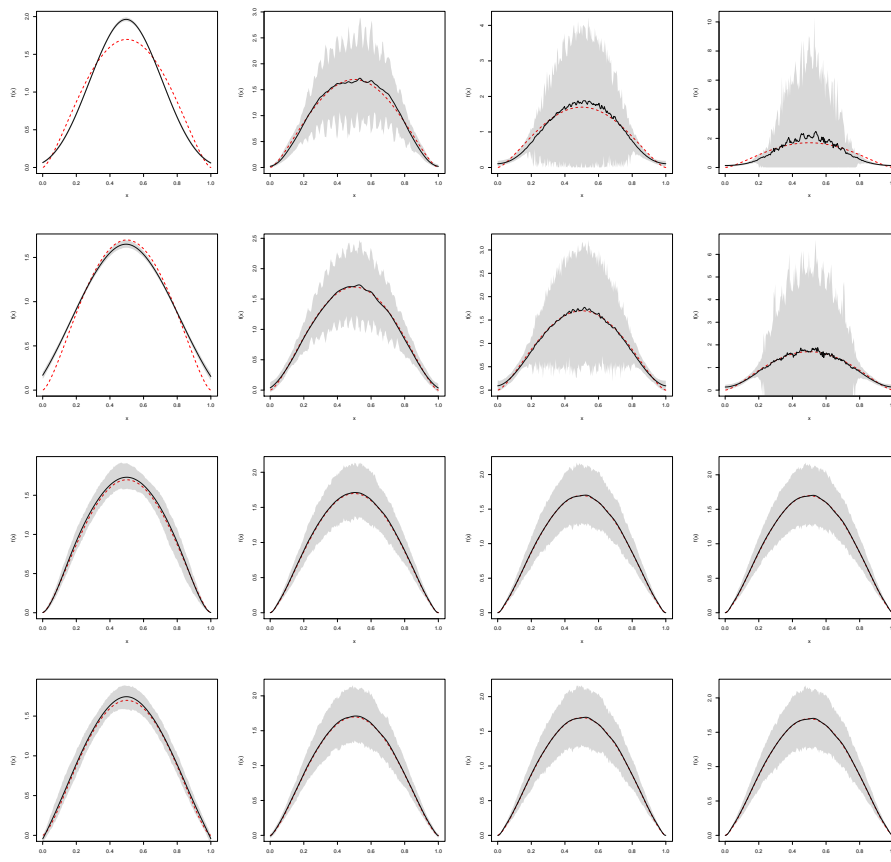


FIG 5. Pointwise average estimates (full lines), with 95% confidence intervals (shaded regions), for the density in ex_1 (dashed lines), with $n = 1,000$. The columns 1–4 are related to the cases where we consider the finest resolution level $J_1 = \lceil p \log_2 n \rceil$, $p = 0.20, 0.45, 0.70, 0.95$, respectively. The k -th row is related to the estimation method m_k , $k = 1, 2, 3, 4$.

3.2. Application

Let us consider the dataset of 2,495 blood alcohol concentrations (BAC) of drivers involved in fatal accidents that occurred in the USA, during the year of 2019. The data was collected from the National Highway Traffic Safety Administration Department of Transportation (www.nhtsa.dot.gov). It is part of The Fatality Analysis Reporting System (FARS), from where we take the brief description of the data (more details in this [link](#)).

The Fatality Analysis Reporting System (FARS) became operational in 1975, and contains data of fatal traffic crashes within the 50 States, the District of Columbia, and Puerto Rico. To be included in FARS, a crash must involve a

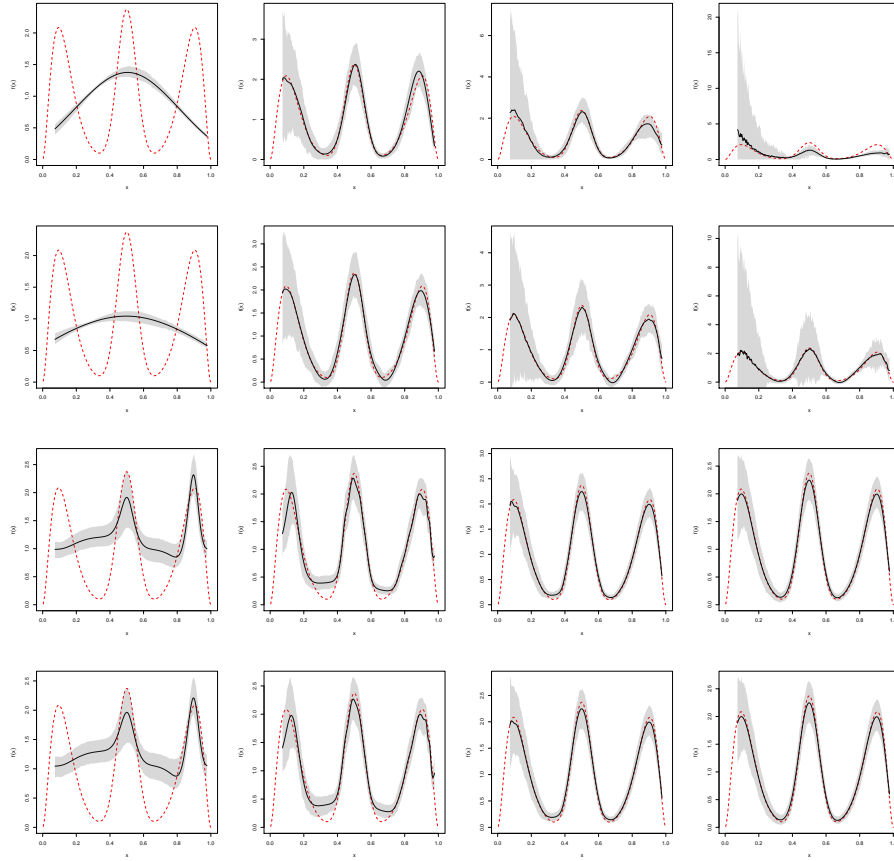


FIG 6. Pointwise average estimates (full lines), with 95% confidence intervals (shaded regions), for the density in ex_2 (dashed lines), with $n = 1,000$. The columns 1–4 are related to the cases where we consider the finest resolution level $J_1 = \lceil p \log_2 n \rceil$, $p = 0.20, 0.45, 0.70, 0.95$, respectively. The k -th row is related to the estimation method m_k , $k = 1, 2, 3, 4$.

motor vehicle traveling on a traffic way customarily open to the public, and must result in the death of a vehicle occupant or a nonoccupant within 30 days of the crash.

BAC here is expressed in grams/100 ml. According to the 2019 FARS/CRSS Coding and Validation Manual (available [here](#)), we consider only fatal crashes where alcohol is involved (according to the police report). Moreover, crashes that are not included in the state highway inventory, not reported or unknown were discarded. Finally, we considered vehicles classified as automobiles, automobiles derivatives, utility vehicles and two-wheel motorcycles.

This is a typical example of a size-biased data. Indeed, as discussed by [16], drunk drivers will more likely be involved in fatal accidents. A histogram is pre-

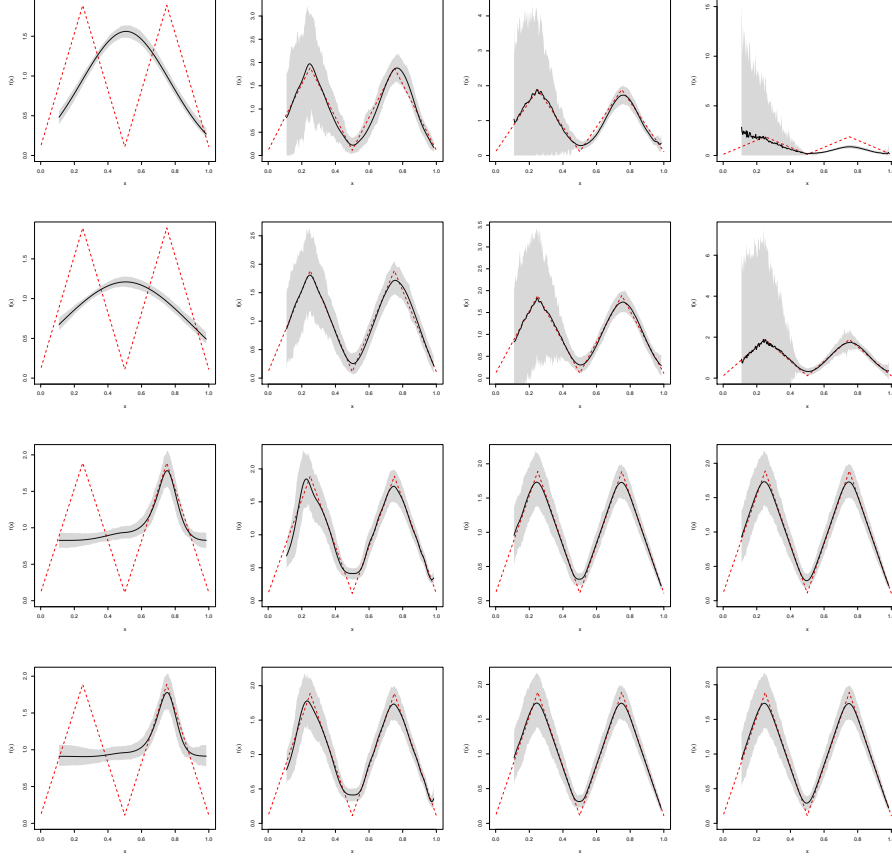


FIG 7. Pointwise average estimates (full lines), with 95% confidence intervals (shaded regions), for the density in ex_3 (dashed lines), with $n = 1,000$. The columns 1–4 are related to the cases where we consider the finest resolution level $J_1 = \lceil p \log_2 n \rceil$, $p = 0.20, 0.45, 0.70, 0.95$, respectively. The k -th row is related to the estimation method m_k , $k = 1, 2, 3, 4$.

sented in Figure 8. The data is mainly concentrated around 0.10–0.25 grams/100 ml. Moreover, the range of observations belongs to the unity interval, with maximum value smaller than 0.55 grams/100 ml, which is not close to one.

The arguments above suggest that the density of interest is biased by an increasing biasing function. Such a function is unknown in practice, and its choice is usually related to historic data, nature of phenomenon and/or common sense [37]. In general, the biasing function should be studied by additional experiments, but in many cases a linear behavior is recommended [16]. Therefore, in this analysis, we assume that

$$w(x) = 0.1 + 0.9x.$$

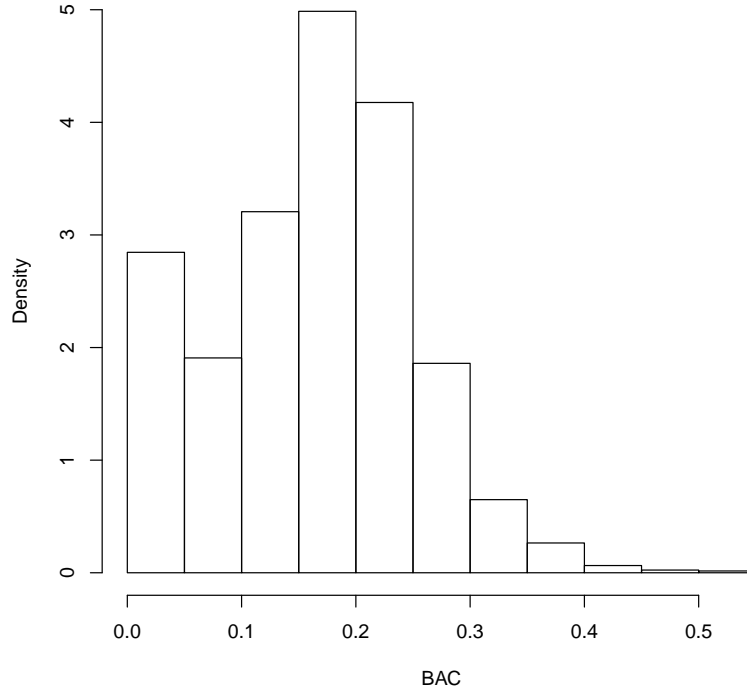


FIG 8. Histogram of the BAC values of drivers involved in fatal accidents in the USA in 2019.

As the data belongs to the unit interval, with its maximum “far” from 1 gram/100 ml, no transformation is needed (Section 2.6). Based on Section 3.1, we consider $J_1 = \lceil 0.45 \log_2 2495 \rceil = 6$ for m_1 and m_2 , and $J_1 = \lceil 0.95 \log_2 2495 \rceil = 11$ for m_3 and m_4 .

Figure 9 shows the four estimates. Methods m_1 and m_2 (orthonormal wavelets) indicate trimodal behavior, with a higher first peak for small amounts of BAC, whilst m_3 and m_4 (warped wavelets), suggest bimodal density, albeit for a tiny bump around 0.5 gram/100 ml for m_4 . The data histogram (Figure 8) and m_1 - m_3 lead us to disregard this bump as some unwarranted feature due to m_4 . Moreover, although not shown here, when m_1 and m_2 are employed with $J_1 = 5$, the second mode seen for $J_1 = 6$ vanishes, bringing all four estimates to a bimodal behavior. Finally, we can see in Figure 9 that some aliasing effect is present: for $m = 2$ vis-a-vis $m = 1$; and for either $m = 2$ or $m = 1$ vis-a-vis $m = 4$ or $m = 3$. Summarizing, we see that warping and/or square-root estimation improves regularization by eliminating aliasing and most residual bumps. Thence, we conclude that m_3 provides the best regularized estimate for the true

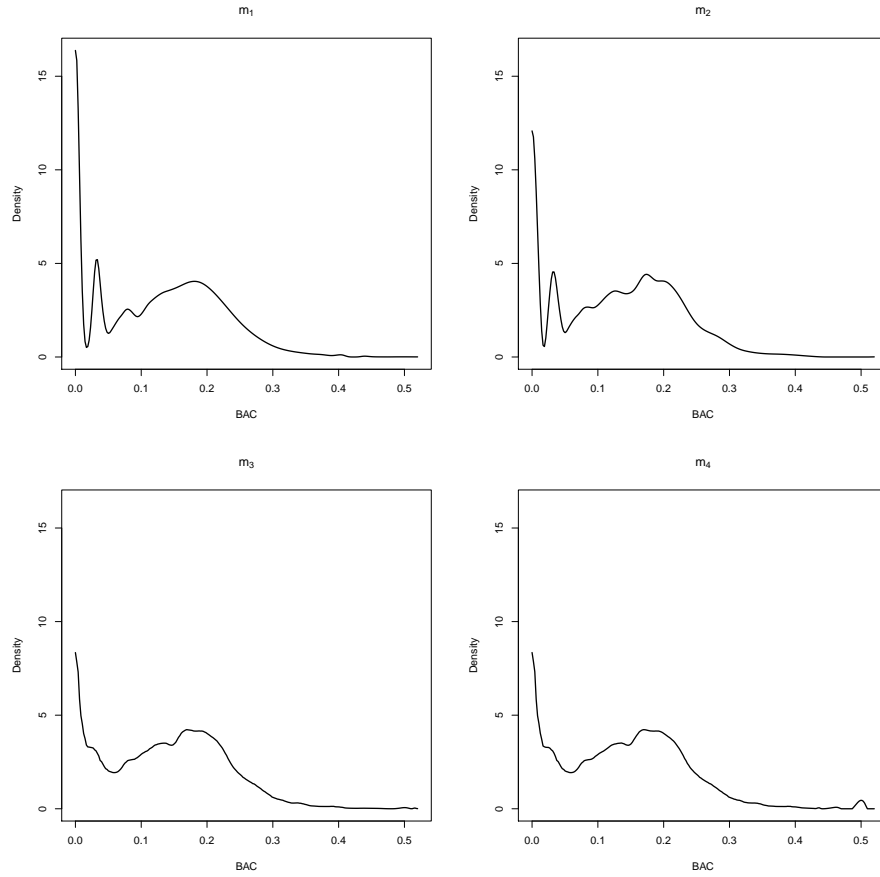


FIG 9. BAC density estimates (top to bottom, left to right): m_1 - $a = 1/2$ and $H(x) = x$; m_2 - $a = 1$ and $H(x) = x$; m_3 - $a = 1/2$ and $H(x) = \hat{G}(x)$; and m_4 - $a = 1$ and $H(x) = \hat{G}(x)$.

density in this application.

4. Conclusions and further remarks

We propose a novel density estimation method in the context of size-biased data. We consider a wavelet-based method to estimate the power of a density of interest in a general framework, where the wavelet basis is allowed to be warped by some cumulative distribution function.

We show that both linear and regularized wavelet estimators are asymptotically consistent and that they attain optimal or near-optimal rates. In numerical studies, we considered four methods of estimation (particular cases of the proposed methodology), which include powers $a = 1/2$ [36] and the usual $a = 1$,

as well as orthonormal and warped wavelet bases. The results indicated that finer resolution levels are better for ordinary orthonormal wavelet bases, whilst coarser resolution levels are better for warped wavelets. Warped wavelet estimators outperform orthonormal estimators, especially in the case of $a = 1/2$.

An issue we did not pursue here, which is left as topic of future research, regards a sharper data-driven estimate for the finest resolution level J_1 .

References

- [1] BORRAJO, M. I., GONZÁLEZ-MANTEIGA, W. and MARTÍNEZ-MIRANDA, M. D. (2017). Bandwidth selection for kernel density estimation with length-biased data. *Journal of Nonparametric Statistics* **29** 636–668.
- [2] BRUNEL, E., COMTE, F. and GUILLOUX, A. (2009). Nonparametric density estimation in presence of bias and censoring. *TEST* **18** 166–194.
- [3] CAI, T. T. and BROWN, L. D. (1998). Wavelet Shrinkage for Nonequispaced Samples. *The Annals of Statistics* **26** 1783–1799.
- [4] CAI, T. T. and BROWN, L. D. (1999). Wavelet estimation for samples with random uniform design. *Statistics & Probability Letters* **42** 313–321.
- [5] CHESNEAU, C. (2010). Wavelet block thresholding for density estimation in the presence of bias. *Journal of the Korean Statistical Society* **39** 43–53.
- [6] CHESNEAU, C., DEWAN, I. and DOOSTI, H. (2012). Wavelet linear density estimation for associated stratified size-biased sample. *Journal of Nonparametric Statistics* **24** 429–445.
- [7] COX, D. R. (1969). Some sampling problems in technology. In *New Developments in Survey Sampling* (N. L. Johnson and H. Smith Jr., eds.) 506–527. Wiley-Interscience, New York.
- [8] CUTILLO, L., DE FEIS, I., NIKOLAIDOU, C. and SAPATINAS, T. (2014). Wavelet density estimation for weighted data. *Journal of Statistical Planning and Inference* **146** 1–19.
- [9] DAUBECHIES, I. and LAGARIAS, J. C. (1991). Two-scale difference equations. I. Existence and global regularity of solutions. *SIAM Journal on Mathematical Analysis* **22** 1388–1410.
- [10] DAUBECHIES, I. and LAGARIAS, J. C. (1992). Two-Scale Difference Equations. II. Local Regularity, Infinite Products of Matrices and Fractals. *SIAM Journal on Mathematical Analysis* **23** 1031–1079.
- [11] DONOHO, D. L., JOHNSTONE, I. M., KERKYACHARIAN, G. and PICARD, D. (1995). Wavelet Shrinkage: Asymptopia? *Journal of the Royal Statistical Society. Series B (Methodological)* **57** 301–369.
- [12] DONOHO, D. L., JOHNSTONE, I. M., KERKYACHARIAN, G. and PICARD, D. (1996). Density estimation by wavelet thresholding. *The Annals of Statistics* **24** 508–539.
- [13] DONOHO, D. L. and JOHNSTONE, J. M. (1994). Ideal spatial adaptation by wavelet shrinkage. *Biometrika* **81** 425–455.
- [14] DOUKHAN, P. (1988). Formes de Toëplitz associées à une analyse multi-échelle. *C. R. Acad. Sci. Paris Série I* **306** 663–666.

- [15] DOUKHAN, P. and LEÓN, J. R. (1990). Déviations quadratique d'estimateurs de densité par projections orthogonales. *C. R. Acad. Sci. Paris Série I Math* **310** 425–430.
- [16] EFROMOVICH, S. (1999). *Nonparametric curve estimation: methods, theory and applications*. Springer series in statistics. Springer, New York.
- [17] EFROMOVICH, S. (2004). Distribution estimation for biased data. *Journal of Statistical Planning and Inference* **124** 1–43.
- [18] EFROMOVICH, S. (2004). Density estimation for biased data. *The Annals of Statistics* **32** 1137–1161.
- [19] EL BARMÍ, H. and SIMONOFF, J. S. (2000). Transformation- based density estimation for weighted distributions. *Journal of Nonparametric Statistics* **12** 861–878.
- [20] FAN, J. and GIJBELS, I. (1996). *Local polynomial modelling and its applications*. Monographs on statistics and applied probability **66**. Chapman & Hall, London.
- [21] GINÉ, E. and GUILLOU, A. (2002). Rates of strong uniform consistency for multivariate kernel density estimators. *Annales de l'Institut Henri Poincaré (B) Probability and Statistics* **38** 907–921.
- [22] GINÉ, E. and NICKL, R. (2009). Uniform limit theorems for wavelet density estimators. *The Annals of Probability* **37** 1605–1646.
- [23] GUO, H. and KOU, J. (2019). Pointwise density estimation based on negatively associated data. *Journal of Inequalities and Applications* **2019** 206.
- [24] GUO, H. and KOU, J. (2019). Pointwise density estimation for biased sample. *Journal of Computational and Applied Mathematics* **361** 444–458.
- [25] HARDLE, W., KERKYACHARIAN, G., PICARD, D. and TSYBAKOV, A. B. (1998). *Wavelets, Approximation and Statistical Applications*. Lecture notes in statistics **129**. Springer, New York.
- [26] JONES, M. C. (1991). Kernel density estimation for length biased data. *Biometrika* **78** 511–519.
- [27] KERKYACHARIAN, G. and PICARD, D. (1992). Density estimation in Besov spaces. *Statistics & Probability Letters* **13** 15–24.
- [28] KERKYACHARIAN, G. and PICARD, D. (1993). Density estimation by kernel and wavelets methods: Optimality of Besov spaces. *Statistics & Probability Letters* **18** 327–336.
- [29] KERKYACHARIAN, G. and PICARD, D. (2004). Regression in Random Design and Warped Wavelets. *Bernoulli* **10** 1053–1105.
- [30] KLEMELÄ, J. (2009). *Smoothing of multivariate data: density estimation and visualization*. Wiley Series in Probability and Statistics. John Wiley & Sons, Hoboken, N.J.
- [31] KOU, J. and GUO, H. (2018). Wavelet density estimation for mixing and size-biased data. *Journal of Inequalities and Applications* **2018** 189.
- [32] MALLAT, S. G. (2008). *A Wavelet Tour of Signal Processing: The Sparse Way*, 3rd ed. Elsevier/Academic Press, Boston.
- [33] MONTORIL, M. H., CHANG, W. and VIDAČOVIĆ, B. (2019). Wavelet-Based Estimation of Generalized Discriminant Functions. *Sankhya B* **81** 318–349.

- [34] MONTORIL, M. H., MORETTIN, P. A. and CHIANN, C. (2018). Wavelet estimation of functional coefficient regression models. *International Journal of Wavelets, Multiresolution and Information Processing* **16** 1850004.
- [35] MORETTIN, P. A., PINHEIRO, A. and VIDAKOVIC, B. (2017). *Wavelets in Functional Data Analysis. SpringerBriefs in Mathematics*. Springer International Publishing, Cham.
- [36] PINHEIRO, A. and VIDAKOVIC, B. (1997). Estimating the square root of a density via compactly supported wavelets. *Computational Statistics & Data Analysis* **25** 399–415.
- [37] RAMÍREZ, P. and VIDAKOVIC, B. (2010). Wavelet density estimation for stratified size-biased sample. *Journal of Statistical Planning and Inference* **140** 419–432.
- [38] RESTREPO, J. M. and LEAF, G. K. (1997). Inner product computations using periodized Daubechies wavelets. *International Journal for Numerical Methods in Engineering* **40** 3557–3578.
- [39] SCOTT, D. W. (2015). *Multivariate density estimation: theory, practice, and visualization*, 2nd ed. *Wiley Series in Probability and Statistics*. John Wiley & Sons, Inc, Hoboken, New Jersey.
- [40] SHEATHER, S. J. and JONES, M. C. (1991). A Reliable Data-Based Bandwidth Selection Method for Kernel Density Estimation. *Journal of the Royal Statistical Society: Series B (Methodological)* **53** 683–690.
- [41] SILVERMAN, B. W. (1978). Weak and Strong Uniform Consistency of the Kernel Estimate of a Density and its Derivatives. *The Annals of Statistics* **6**.
- [42] TENZER, Y., MANDEL, M. and ZUK, O. (2021). Testing Independence Under Biased Sampling. *Journal of the American Statistical Association* 1–13.
- [43] VARDI, Y. (1982). Nonparametric Estimation in the Presence of Length Bias. *The Annals of Statistics* **10** 616–620.
- [44] VIDAKOVIC, B. (1999). *Statistical modeling by wavelets. Wiley series in probability and mathematical statistics. Applied probability and statistics section*. Wiley, New York.
- [45] WANG, J., WANG, M. and ZHOU, Y. (2013). Nonlinear wavelet density estimation for biased data in Sobolev spaces. *Journal of Inequalities and Applications* **2013** 308.
- [46] YU, Y. (2020). Pointwise Wavelet Estimation of Density Function with Change-Points Based on NA and Biased Sample. *Results in Mathematics* **75** 146.
- [47] YU, Y. and LIU, X. (2020). Pointwise wavelet change-points estimation for dependent biased sample. *Journal of Computational and Applied Mathematics* **380** 112986.

Appendix A: Proofs of the theoretical results in Section 2.4

We give here the proofs of the results from Section 2.4. By assumptions (a2) and (a3),

$$w(y) \asymp 1, \quad (14)$$

$$h(y) \asymp 1, \quad (15)$$

respectively. Also, note that assumptions (a1)-(a2) guarantee

$$\mu \asymp 1, \quad (16)$$

$$g(y) \asymp 1, \quad (17)$$

From (14),

$$\hat{\mu} = \frac{1}{n} \sum_{i=1}^n w^{-1}(Y_i) \asymp 1. \quad (18)$$

We need the following lemma.

Lemma 1. *Under the assumptions (a1)-(a4), for $k = 0, 1, \dots, 2^{J_0} - 1$,*

$$\mathbb{E} |\hat{c}_{J_0 k} - c_{J_0 k}|^2 \lesssim D_n \mathbb{1}_{\{a \neq 1\}} + n^{-1},$$

where D_n is a positive sequence such that $\sup_{y \in [0,1]} |\hat{g}(y) - g(y)|^2 \lesssim D_n$ a.s.

Proof of Theorem 1. Analogous to the proof of Theorem 2 below. \square

Proof of Theorem 2. Initially, observe that the convergence of $\hat{f}_{J_0}^a$ is equivalent to the convergence of $\hat{r}_{J_0}^a$, where r^a is defined in (3). In fact, by assumption (a3), it is easy to see that

$$\|f^a\|^2 \asymp \|r^a\|^2. \quad (19)$$

Let us denote $\rho_j = \|r_j^a - r^a\|$, for a positive integer j . Since, by (a4), r^a is analyzed by an orthonormal basis, it is easy to see that

$$\mathbb{E} \|\hat{r}_{J_0}^a - r^a\|^2 = \mathbb{E} \|\hat{r}_{J_0}^a - r_{J_0}^a\|^2 + \rho_{J_0}^2.$$

By (a1) we have [38]

$$\rho_{J_0}^2 \lesssim 2^{-2mJ_0}. \quad (20)$$

By (a4) the basis is orthonormal. Therefore, by Parseval's identity and Lemma 1,

$$\begin{aligned} \mathbb{E} \|\hat{r}_{J_0}^a - r_{J_0}^a\|^2 &= \sum_{k=0}^{2^{J_0}-1} \mathbb{E} |\hat{c}_{J_0 k} - c_{J_0 k}|^2 \lesssim \sum_{k=0}^{2^{J_0}-1} (D_n + n^{-1}) \\ &= 2^{J_0} D_n + \frac{2^{J_0}}{n}. \end{aligned} \quad (21)$$

The desired result follows from (19)-(21). \square

Proof of Corollary 1. Observe that by Theorem 3,

$$D_n \lesssim \frac{J_0 2^{J_0}}{n} + 2^{-2mJ_0}.$$

Hence,

$$\begin{aligned} 2^{J_0} D_n + \frac{2^{J_0}}{n} + 2^{-2mJ_0} &\lesssim \frac{J_0 2^{2J_0}}{n} + 2^{-(2m-1)J_0} + \frac{2^{J_0}}{n} + 2^{-2mJ_0} \\ &\lesssim \frac{J_0 2^{2J_0}}{n} + 2^{-(2m-1)J_0}, \end{aligned}$$

which provides the desired result. \square

Proof of Theorem 4. Still using r^a as defined in (3), observe that $\rho_j = \|r_j^a - r^a\| = \sum_{j=J_1}^{+\infty} \sum_{k=0}^{2^j-1} d_{jk}$. By Parseval's identity, it is easy to see that

$$\mathbb{E} \|\tilde{r}_{J_1}^a - r^a\|^2 = \sum_{k=0}^{2^{J_0}-1} \mathbb{E} (\hat{c}_{J_0 k} - c_{J_0 k})^2 + \sum_{j=J_0}^{J_1-1} \sum_{k=0}^{2^j-1} \mathbb{E} (\tilde{d}_{jk} - d_{jk})^2 + \rho_{J_1}. \quad (22)$$

Since $0 \leq \lambda_{jk} \leq 1$, the second term of the right hand side of the inequality above is bounded by

$$\begin{aligned} \sum_{j=J_0}^{J_1-1} \sum_{k=0}^{2^j-1} \mathbb{E} (\tilde{d}_{jk} - d_{jk})^2 &= \sum_{j=J_0}^{J_1-1} \sum_{k=0}^{2^j-1} \mathbb{E} (\lambda_{jk} \hat{d}_{jk} - d_{jk})^2 \\ &= \sum_{j=J_0}^{J_1-1} \sum_{k=0}^{2^j-1} \mathbb{E} (\lambda_{jk} \hat{d}_{jk} - \lambda_{jk} d_{jk} + \lambda_{jk} d_{jk} - d_{jk})^2 \\ &\leq 2 \sum_{j=J_0}^{J_1-1} \sum_{k=0}^{2^j-1} \mathbb{E} [\lambda_{jk}^2 (\hat{d}_{jk} - d_{jk})^2] \\ &\quad + 2 \sum_{j=J_0}^{J_1-1} \sum_{k=0}^{2^j-1} \mathbb{E} [(\lambda_{jk} - 1)^2 d_{jk}^2] \\ &\leq 2 \sum_{j=J_0}^{J_1-1} \sum_{k=0}^{2^j-1} \mathbb{E} (\hat{d}_{jk} - d_{jk})^2 + 2 \sum_{j=J_0}^{J_1-1} \sum_{k=0}^{2^j-1} d_{jk}^2 \\ &= 2 \left[\sum_{j=J_0}^{J_1-1} \sum_{k=0}^{2^j-1} \mathbb{E} (\hat{d}_{jk} - d_{jk})^2 + \rho_{J_0}^2 - \rho_{J_1}^2 \right], \end{aligned} \quad (23)$$

because $\sum_{j=J_0}^{J_1-1} \sum_{k=0}^{2^j-1} d_{jk}^2 = \rho_{J_0}^2 - \rho_{J_1}^2$.

Therefore, (22), (23) and Theorem 1 ensure that

$$\mathbb{E} \|\tilde{r}_{J_1}^a - r^a\|^2 \lesssim \sum_{k=0}^{2^{J_0}-1} \mathbb{E} (\hat{c}_{J_0 k} - c_{J_0 k})^2 + \sum_{j=J_0}^{J_1-1} \sum_{k=0}^{2^j-1} \mathbb{E} (\hat{d}_{jk} - d_{jk})^2 + \rho_{J_1}. \quad (24)$$

The last term above comes from the fact that $\rho_{J_0} \asymp \rho_{J_1}$, because $2^{J_0} \asymp 2^{J_1}$, as stated in the above-mentioned theorem.

The desired result is yielded by (19). \square

Proofs of Theorem 5 and Corollary 2. The proofs of these results are similar to the proof of Theorem 4 presented above. \square

Proof of Lemma 1. Let us focus initially on the case where $a \neq 1$. Then the estimator of the wavelet coefficients in (6) can be written as

$$\begin{aligned}\hat{c}_{J_0k} &= \frac{\hat{\mu}^a}{n} \sum_{i=1}^n \frac{\phi_{J_0k}[H(Y_i)]h(Y_i)\hat{g}^{a-1}(Y_i)}{w^a(Y_i)} \\ &= \frac{\hat{\mu}^a}{n} \sum_{i=1}^n \frac{\phi_{J_0k}[H(Y_i)]h(Y_i)}{w^a(Y_i)} [\hat{g}^{a-1}(Y_i) - g^{a-1}(Y_i)] \\ &\quad + \frac{\hat{\mu}^a}{n} \sum_{i=1}^n \frac{\phi_{J_0k}[H(Y_i)]h(Y_i)g^{a-1}(Y_i)}{w^a(Y_i)}.\end{aligned}$$

Thus,

$$\begin{aligned}\hat{c}_{J_0k} - c_{J_0k} &= \frac{\hat{\mu}^a}{n} \sum_{i=1}^n \frac{\phi_{J_0k}[H(Y_i)]h(Y_i)}{w^a(Y_i)} [\hat{g}^{a-1}(Y_i) - g^{a-1}(Y_i)] \\ &\quad + \frac{\hat{\mu}^a}{n} \sum_{i=1}^n \frac{\phi_{J_0k}[H(Y_i)]h(Y_i)g^{a-1}(Y_i)}{w^a(Y_i)} - c_{J_0k} \\ &= \frac{\hat{\mu}^a}{n} \sum_{i=1}^n \frac{\phi_{J_0k}[H(Y_i)]h(Y_i)}{w^a(Y_i)} [\hat{g}^{a-1}(Y_i) - g^{a-1}(Y_i)] \\ &\quad + \left(\frac{\hat{\mu}}{\mu}\right)^a \left[\frac{\mu^a}{n} \sum_{i=1}^n \frac{\phi_{J_0k}[H(Y_i)]h(Y_i)g^{a-1}(Y_i)}{w^a(Y_i)} - c_{J_0k} \right] \\ &\quad + c_{J_0k} \hat{\mu}^a \left(\frac{1}{\mu^a} - \frac{1}{\hat{\mu}^a} \right),\end{aligned}$$

which implies

$$\begin{aligned}\mathbb{E} |\hat{c}_{J_0k} - c_{J_0k}|^2 &\lesssim \mathbb{E} \left| \frac{\hat{\mu}^a}{n} \sum_{i=1}^n \frac{\phi_{J_0k}[H(Y_i)]h(Y_i)}{w^a(Y_i)} [\hat{g}^{a-1}(Y_i) - g^{a-1}(Y_i)] \right|^2 \\ &\quad + \mathbb{E} \left| \left(\frac{\hat{\mu}}{\mu}\right)^a \left[\frac{\mu^a}{n} \sum_{i=1}^n \frac{\phi_{J_0k}[H(Y_i)]h(Y_i)g^{a-1}(Y_i)}{w^a(Y_i)} - c_{J_0k} \right] \right|^2 \\ &\quad + \mathbb{E} \left| c_{J_0k} \hat{\mu}^a \left(\frac{1}{\mu^a} - \frac{1}{\hat{\mu}^a} \right) \right|^2 \\ &\equiv I_1 + I_2 + I_3.\end{aligned}\tag{25}$$

Beginning with I_1 , by (17) it is easy to see that g^a is Lipschitz, satisfying

$$|\hat{g}^{a-1}(y) - g^{a-1}(y)| \lesssim |\hat{g}(y) - g(y)| \quad \forall y \in [0, 1] \quad a.s. \quad (26)$$

Hence, since Y_1, \dots, Y_n are i.i.d., by (18) and due to (26),

$$\begin{aligned} I_1 &= \mathbb{E} \left| \hat{\mu}^a \frac{\phi_{J_0 k}[H(Y)]h(Y)}{w^a(Y)} [\hat{g}^{a-1}(Y) - g^{a-1}(Y)] \right|^2 \\ &\asymp \mathbb{E} \left| \frac{\phi_{J_0 k}[H(Y)]h(Y)}{w^a(Y)} [\hat{g}^{a-1}(Y) - g^{a-1}(Y)] \right|^2 \\ &\lesssim \mathbb{E} \left| \frac{\phi_{J_0 k}[H(Y)]h(Y)}{w^a(Y)} [\hat{g}(Y) - g(Y)] \right|^2. \end{aligned}$$

If there is a positive sequence D_n such that

$$\sup_{y \in [0, 1]} |\hat{g}(y) - g(y)|^2 \lesssim D_n \quad a.s.,$$

then,

$$I_1 \lesssim D_n \mathbb{E} \left| \frac{\phi_{J_0 k}[H(Y)]h(Y)}{w^a(Y)} \right|^2 \asymp D_n \int_0^1 \phi_{J_0 k}^2(y) dy = D_n, \quad (27)$$

where the second inequality comes from (14)-(15), and the third inequality is due to the fact that $\int_0^1 \phi_{J_0 k}^2(y) dy = 1$ [38].

In the analysis of I_2 , let us denote

$$\xi_i = \frac{\mu^a \phi_{J_0 k}[H(Y_i)]h(Y_i)g^{a-1}(Y_i)}{w^a(Y_i)} - c_{J_0 k},$$

for $i = 1, 2, \dots, n$. It is immediate that $\xi_1, \xi_2, \dots, \xi_n$ are i.i.d. Moreover, $\mathbb{E}(\xi_i) = 0$ and $\text{Var}(\xi_i) = 1$. In fact, the zero mean comes from (5) and

$$\begin{aligned} \text{Var}(\xi_i) &= \mathbb{E}(\xi_i^2) \\ &= \mathbb{E} \left[\frac{\mu^a \phi_{J_0 k}[H(Y_i)]h(Y_i)g^{a-1}(Y_i)}{w^a(Y_i)} - c_{J_0 k} \right]^2 \\ &\lesssim \mathbb{E} \left[\frac{\mu^a \phi_{J_0 k}[H(Y_i)]h(Y_i)g^{a-1}(Y_i)}{w^a(Y_i)} \right]^2 + c_{J_0 k}^2 \\ &\lesssim \mathbb{E} \left[\frac{\mu^a \phi_{J_0 k}[H(Y_i)]h(Y_i)g^{a-1}(Y_i)}{w^a(Y_i)} \right]^2 \\ &\asymp \int_0^1 \phi_{J_0 k}^2[H(y)]h(y) dy \\ &= \int_0^1 \phi_{J_0 k}^2(x) dx = 1, \end{aligned} \quad (28)$$

where the fourth inequality comes from the fact that

$$\begin{aligned} c_{J_0k}^2 &= \left\{ \mathbb{E} \left[\mu^a \phi_{J_0k} [H(Y_i)] h(Y_i) g^{a-1}(Y_i) / w^a(Y_i) \right] \right\}^2 \\ &\leq \mathbb{E} \left[\mu^a \phi_{J_0k} [H(Y_i)] h(Y_i) g^{a-1}(Y_i) / w^a(Y_i) \right]^2 \end{aligned}$$

and the fifth from (14)–(17). Therefore, by (16) and (18), and because of (28), we have that

$$I_2 \asymp \text{Var} \left(n^{-1} \sum_{i=1}^n \xi_i \right) = n^{-1} \text{Var}(\xi_1) \lesssim n^{-1}. \quad (29)$$

Finally, note that, by (18),

$$I_3 \lesssim \mathbb{E} \left| \hat{\mu}^a \left(\frac{1}{\mu^a} - \frac{1}{\hat{\mu}^a} \right) \right|^2 \asymp \mathbb{E} \left| \frac{1}{\mu^a} - \frac{1}{\hat{\mu}^a} \right|^2. \quad (30)$$

Because of (16) and (18), we have that $1/\mu^a$ and $1/\hat{\mu}^a$ are Lipschitz continuous functions of $1/\mu$ and $1/\hat{\mu}$, respectively. Therefore,

$$\left| \frac{1}{\mu^a} - \frac{1}{\hat{\mu}^a} \right| \lesssim \left| \frac{1}{\mu} - \frac{1}{\hat{\mu}} \right| \quad a.s.$$

Hence, by (30),

$$I_3 \lesssim \mathbb{E} \left| \frac{1}{\mu} - \frac{1}{\hat{\mu}} \right|^2 \lesssim n^{-1}. \quad (31)$$

The last inequality is verified as in the end of Proposition 4.1's proof [5].

Therefore, (25), (27), (29) and (31) ensure that, for the case where $a \neq 1$,

$$\mathbb{E} |\hat{c}_{J_0k} - c_{J_0k}|^2 \lesssim D_n + n^{-1}. \quad (32)$$

The case where $a = 1$ is analogous but simpler. Observe that, when $a = 1$, $\hat{g}^{a-1}(y) = 1$ and $g^{a-1}(y) = 1$ for $y \in [0, 1]$. Therefore, in (25), the term I_1 becomes null and the terms I_2 and I_3 are simplified without changing the upper bounds in (29) and (31), respectively. Thus, for $a = 1$,

$$\mathbb{E} |\hat{c}_{J_0k} - c_{J_0k}|^2 \lesssim n^{-1}. \quad (33)$$

Hence, (32) and (33) yield the desired result. \square